Applied Energy 254 (2019) 113624

Contents lists available at ScienceDirect

Applied Energy

journal homepage: www.elsevier.com/locate/apenergy

Cycle design and optimization of pressure swing adsorption cycles for pre-combustion CO_2 capture

Sai Gokul Subraveti[a], Kasturi Nagesh Pai[a], Ashwin Kumar Rajagopalan[b], Nicholas Stiles Wilkins[a], Arvind Rajendran[a,*], Ambalavan Jayaraman[c], Gokhan Alptekin[c]

[a] Department of Chemical and Materials Engineering, University of Alberta, 12th Floor, Donadeo Innovation Centra for Engineering (ICE), 9211-116 Street, Edmonton, Alberta T6G1H9, Canada
[b] Institute of Process Engineering, ETH Zurich, 8092 Zurich, Switzerland
[c] TDA Research Inc., Wheat Ridge, CO 80033, USA

HIGHLIGHTS

- Novel steam-purge pressure swing adsorption cycles for pre-combustion CO_2 capture.
- Three cycles meet regulatory targets of CO_2 purity > 95% and recovery > 90%.
- Genetic-algorithm based optimization to minimize energy and maximize productivity.
- Parasitic Energy: 95.7 kWh_e/tonne CO_2 cap, productivity: 3.3 mol CO_2 cap/m^3 ads/s.

ARTICLE INFO

Keywords:
Pre-combustion carbon capture
Pressure swing adsorption
Multi-objective optimization
Modeling
Genetic algorithm
Dynamic simulation

ABSTRACT

Novel pressure-swing adsorption (PSA) cycles were developed based on patented TDA AMS-19 (activated carbon) adsorbent for pre-combustion CO_2 capture in integrated gasification combined cycle (IGCC) power plants. A variety of cycles comprising of counter-current blowdown, pressure equalization, steam purge and light product pressurization steps were designed and simulated using an in-house one dimensional detailed model. Full process optimization studies were performed for all cycles to evaluate their feasibility for pre-combustion CO_2 capture. The CO_2 purity and recovery Pareto fronts obtained using the multi-objective optimization were used to assess their ability to simultaneously achieve high CO_2 purity (> 95%) and recovery (> 90%). The cycles that achieved the purity-recovery (95–90%) requirements were subjected to energy-productivity optimizations under the constraints of CO_2 purity and recovery. Three cycle designs were ranked in terms of lowest energy consumption at 95% CO_2 purities and 90% CO_2 recoveries. It was found that a 10-step cycle with three pressure equalization steps achieved a minimum energy consumption of 95.7 kWh_e/tonne of CO_2 captured at a productivity of 3.3 mol CO_2 captured/m^3 adsorbent/s.

1. Introduction

Climate change is proceeding faster each year with increasing usage of fossil fuels [1]. Anthropogenic greenhouse gas emissions, particularly CO_2, contribute to climate change. Currently, about 35% of anthropogenic CO_2 emissions come from the energy and power sectors [1]. One possible way to mitigate climate change is to reduce CO_2 emissions; this could be possible if power generation were switched to renewable sources or fossil fuel generated power becomes carbon-neutral. Reduced CO_2 emissions can be achieved with carbon dioxide capture and storage (CCS), the process of separating CO_2 from a bulk gas stream, usually from an industrial power plant, and storing the captured CO_2 underground [2]. There are a few ways to implement CCS in a fossil fuel-based power plant. Post-combustion CO_2 capture separates the CO_2 after combustion of the fuel. Post-combustion flue gas contains mostly N_2, 5–15 mol% CO_2 and about 8–10 mol% H_2O [3]. Post-combustion CO_2 capture has been studied extensively, since it can be retrofitted to existing power plants. Since the concentration of CO_2 in post-combustion capture is very low (5–15 mol% CO_2), the separation becomes difficult. An alternative is pre-combustion CO_2 capture, which separates CO_2 from a syngas that is generated from the gasification of coal in an integrated gasification combined cycle (IGCC) power plant,

* Corresponding author.
E-mail address: arvind.rajendran@ualberta.ca (A. Rajendran).

https://doi.org/10.1016/j.apenergy.2019.113624
Received 28 March 2019; Received in revised form 21 July 2019; Accepted 24 July 2019
Available online 07 August 2019

Nomenclature

Roman symbols

$C_{p,a}$	specific heat capacity of the adsorbed phase [J mol^{-1} K^{-1}]
$C_{p,g}$	specific heat capacity of the gas phase [J mol^{-1} K^{-1}]
$C_{p,s}$	specific heat capacity of the adsorbent [J kg^{-1} K^{-1}]
$C_{p,w}$	specific heat capacity of the column wall [J kg^{-1} K^{-1}]
D_L	axial dispersion [m^2 s^{-1}]
E_c	electrical energy required for CO_2 compression [kWh_e]
E_s	electrical energy from the steam usage [kWh_e]
E_h	electrical energy required for H_2 compression [kWh_e]
En	electrical energy consumption [kWh_e $tonne^{-1}$]
h	specific enthalpy of saturated steam [kJ kg^{-1}]
H	specific enthalpy [kJ kg^{-1}]
h_{in}	inside heat transfer coefficient [J m^{-2} K^{-1} s^{-1}]
h_{out}	outside heat transfer coefficient [J m^{-2} K^{-1} s^{-1}]
J	objective function
k	adsorption equilibrium constant [Pa^{-1}]
k_{avg}	mass transfer coefficient [s^{-1}]
K_z	effective gas thermal conductivity [J m^{-1} K^{-1} s^{-1}]
L	column length [m]
m	mass flow rate [kg s^{-1}]
n	molar flow rate [kmol s^{-1}]
N	number of stages [–]
p	partial pressure [Pa]
P	pressure [Pa]
P_H	high pressure in cycle simulation [Pa]
P_I	intermediate pressure in cycle simulation [Pa]
P_L	low pressure in cycle simulation [Pa]
Pu	purity [%]
Pr	productivity [mol CO_2 m^{-3} s^{-1}]
q	solid phase loading [mol kg^{-1}]
q^*	equilibrium solid phase loading [mol kg^{-1}]
q^*_{sat}	temperature dependent saturation solid phase loading [mol kg^{-1}]
R	universal gas constant [Pa m^3 mol^{-1} K^{-1}]
r_{in}	column inner radius [m]
r_{out}	column outer radius [m]
r_p	particle radius [m]
Re	recovery [%]
s	Sips isotherm exponent [–]
t	time [s]
T	temperature [K]
T_a	ambient temperature [K]
T_w	column wall temperature [K]
v	interstitial velocity [m s^{-1}]
W	work done [kJ]
y	gas phase composition [–]
z	axial coordinate [m]

Greek symbols

γ	adiabatic constant [–]
ε	bed voidage [–]
η	efficiency [–]
θ	Sips isotherm parameter [Pa^{-1}]
λ	penalty factor [–]
μ	fluid viscosity [kg m^{-1} s^{-1}]
ρ_s	adsorbent particle density [kg m^{-3}]
ρ_w	wall density [kg m^{-3}]
ϕ	Sips isotherm parameter [kJ mol^{-1}]
φ	Sips isotherm parameter [kJ mol^{-1}]
χ	empirical coefficients [–]
ψ	penalty factor [-]
ω	Sips isotherm parameter [mol kg^{-1}]

Acronyms

ADS	adsorption step
CAI	California Analytical Instruments
CCS	carbon dioxide capture and storage
CnBLO	counter-current blowdown step
CoBLO	co-current blowdown step
CSS	cyclic steady-state
IGCC	integrated gasification combined cycle
LDF	linear driving force
LPP	light product pressurization
ODE	ordinary differential equation
PDE	partial differential equation
PREQ	pressure equalization step
PRESS	feed pressurization step
PSA	pressure-swing adsorption
PUR	purge step

Subscripts

c	compression
h	hydrogen
H	high
i	component
I	intermediate
in	inlet stream
L	low
out	outlet stream
pump	pump
s	steam

as shown in Fig. 1. The processed syngas downstream of the water-gas shift reactor, after desulfurization mainly comprises of CO_2 and H_2. This allows for the separation of CO_2 before the combustion of the fuel (H_2). The feed concentration of a typical pre-combustion gas stream is about 15–60 mol% CO_2 with the balance being H_2 and some diluent, typically H_2O or N_2, at 20–70 bar total pressure [4]. The captured CO_2 needs to be compressed to 150 bar to transport it to a storage site [5]. Several pilot-scale and commercial-scale CO_2 capture units are operational around the world [6–8]. The Kemper project was the first large-scale pre-combustion CO_2 capture demonstrator that was built for an IGCC plant. However, this project was abandoned due to technical and financial reasons. While several other pilot plants are currently operational, the need to improve energy efficiency of these processes has been emphasized in the literature. It is worth noting that pre-combustion capture where the CO_2 partial pressure is much higher than the case of post-combustion capture, provides an attractive opportunity for commercialization [6]. The current commercial technology for pre-combustion CO_2 capture is liquid absorption using amines [7]. However, since the parasitic energy from this process is quite high, other separation technologies are being explored.

Pressure-swing adsorption (PSA) processes have gained wide attention as the potential separation technique owing to the desirable pre-combustion CO_2 capture conditions and low energy requirements [9–12]. In addition, they have also been extensively considered for obtaining ultra high purity H_2 along with CO_2 capture [13–18]. A PSA process exploits the potential of certain solids, e.g., zeolites, carbons, metal-organic frameworks, to selectively adsorb a component from a gas mixture [19]. The selectivity can arise either from differences in

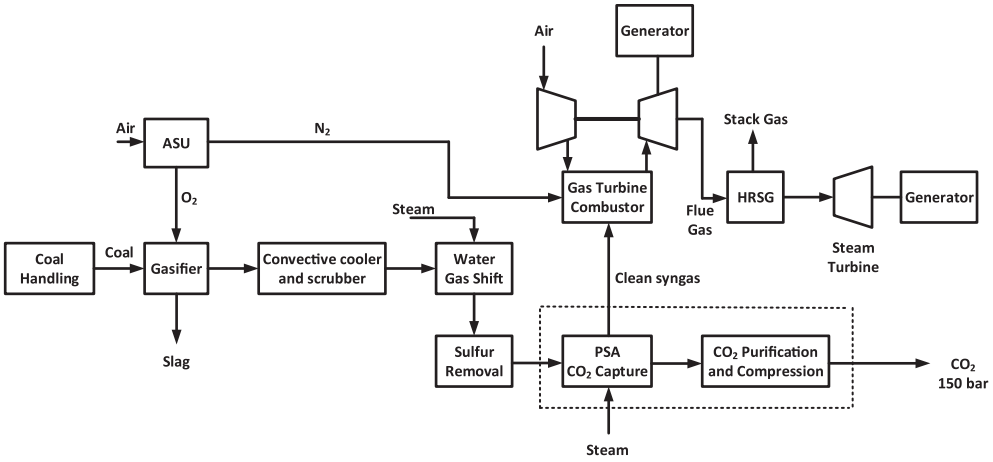

Fig. 1. Schematic of an IGCC power plant. The dotted box represents the scope of the current work. ASU is the air separation unit and HRSG is heat recovery steam generator.

affinity of the gases to the solid surface (equilibrium selectivity) or due to the differences in the rate of adsorption (kinetic selectivity). A PSA process consists of two key steps: Adsorption: performed at high pressure; and Desorption: performed at low pressures. Often, the use of these two steps alone does not result in high purity and recovery of the target product. Hence, additional steps such as purge, blowdown and pressure equalization are added to improve the process performance. This "modularity" provides the possibility of synthesizing several unique cycle configurations that can cater to the specific separation problem. These processes are cyclic and operate under unsteady-state conditions. There are no straightforward design methods and numerical simulations are used to design and optimize these processes. PSA processes are commercialized for H_2 purification in refineries, air separation, CH_4 purification, gas drying etc [20]. Most PSA-based CO_2 capture fall under the category of equilibrium separations. Further, in both pre- and post-combustion capture, CO_2 is typically the strongly adsorbed component compared to the other major component (N_2 in post-combustion and H_2 in pre-combustion).

Pre-combustion CO_2 capture by PSA process has gained attention in the recent years. Air Products demonstrated a vacuum-swing adsorption (VSA) technology for capturing CO_2 in a H_2 purification facility at Port Arthur, Texas, proving that adsorption techniques can be considered for large-scale implementation [21]. Casas et al. presented a parametric study based on a 10-step PSA cycle using an activated carbon for pre-combustion CO_2 capture [9]. The performance of the activated carbon was also modeled and validated with dynamic column breakthrough experiments [22]. The constituent steps in the 10-step cycle were: feed pressurization, adsorption, three pressure equalization donor steps, co-current blowdown, counter-current feed purge and finally three pressure equalization receiver steps [9]. Riboldi et al. designed adsorption-based process that yielded 98.9 mol% CO_2 purity and 89.7 mol% CO_2 recovery and they showed that the adsorption-based process performed similar to liquid amine absorption in terms of energy efficiency [10]. This PSA cycle had 12 steps: feed pressurization, adsorption, 4 pressure equalization donor steps, co-current blowdown, counter-current purge and four pressure equalization receiver steps [10]. It was further demonstrated that the 12-step cycle used slightly more energy than a similar liquid amine absorption process; however, the pre-combustion process used less energy than the post-combustion processes that were evaluated [11]. Agarwal et al. developed a superstructure based approach to determine the optimal cycle and operating conditions to purify CO_2 and H_2 simultaneously [12]. Agarwal et al. were able to achieve H_2 and CO_2 purities up to 99 and 96 mol%, respectively, with CO_2 recoveries up to 92% [12]. Activated carbons are by far the most used adsorbents in the literature for pre-combustion carbon capture [9–11,22,23]. This is due to their hydrophobic nature and high CO_2/H_2 selectivity at elevated pressures [24,25]. A table summarizing some of the key PSA-based pre-combustion capture studies is provided in the supporting information (see Table S1).

The main challenges in developing adsorption processes for pre-combustion CO_2 capture can be summarized as follows: 1. Development of an adsorbent that can sustain operation under harsh process conditions, viz., high temperature, pressure, repeated cycling and the use of steam; 2. Development of PSA cycles that can achieve US-Department of Energy (US-DOE) targets of CO_2 Purity > 95% and recovery > 90%; 3. Estimation of the parasitic energy consumption and productivity of these processes through rigorous process optimization; and 4. Demonstration under real world conditions. A summary of some relevant conditions provided in the supporting information, shows that very few studies manage to achieve US-DOE targets (see Table S1 in the supporting information). In addition, it is difficult to find reliable information about the energy consumption and productivity of these processes which are vital for systems level studies. Hence, there is an acute need to investigate these processes, and develop new ones, that will allow the advancement of this technology.

The objective of this study is to design a variety of PSA processes with low energy consumption for pre-combustion CO_2 capture within an IGCC power plant. It is worth mentioning that the current study was conducted based on the assumption that the syngas feed comprises CO_2 and H_2. The adsorbent material used was an activated carbon called TDA AMS-19 produced by TDA Research Inc. (Wheat Ridge, CO, USA) [26]. To this end, the characterization of the adsorption equilibria for TDA AMS-19 was performed. Based on the adsorption equilibria, process design of six different PSA cycles were carried out and their performances were evaluated using detailed PSA process models. Subsequently, the cycles were subjected to rigorous multi-objective optimizations to determine the cycle with the lowest energy requirements. In this work, we demonstrate how it is possible to start from a simple cycle and build complex ones through careful analysis of the impact of each step coupled with rigorous optimization techniques. Three new cycles, not reported earlier in the literature, have been shown to satisfy US-DOE targets and their merits, in terms of energy consumption and productivity, are evaluated through multi-objective optimization. The maximum productivity obtained in this study was 85% higher than those found in the literature [9].

2. Adsorbent testing and adsorption equilibria

2.1. Adsorbent testing

The adsorbent used in this study, named TDA AMS-19, an activated carbon that has a BET surface area of 401 m^2/g and a DFT micropore

volume of 0.17 cc/g. The adsorbent was tested extensively at TDA Research Inc. for its stability. For the long-term testing, 1.3L of the adsorbent was packed in a column and subjected to a series of cycles. The feed was a simulated synthesis gas with the following molar composition $H_2/CO_2/H_2O/CO$: 15/48.1/36.3/0.6% at 35.5 bar and 240 °C. A simple four-step process was used for the test: 1. Introduce feed gas at 35.5 bar; 2. Depressurize to 20.6 bar; 3. Purge with a gas containing a 50/50 mixture of H_2 and H_2O in order to mimic the partial pressure of water in the actual process; and 4. Pressurize with feed. Each cycle lasted for ≈ 25 min. A total of > 11,650 such cycles were performed. Based on the flow and composition measurements, the CO_2 working capacity was measured. During this campaign, various regeneration and purge methods were tested. Over the extended period of time, the adsorbent showed excellent stability with the CO_2 capacity being maintained at ≈ 8 wt.% (1.8 mol CO_2/kg ads). The results of the long term testing are provided in the supporting information (see Fig. S2) and in the patent document [26].

2.2. Adsorption Equilibria

Determination of adsorption equilibria is a key step for performing process simulation and optimization. CO_2 isotherms on TDA AMS-19 were obtained by performing dynamic column breakthrough experiments at 180°C, 240°C and 300°C between 1 bar and 40 bar total pressure. The CO_2 concentration was measured using two analyzers, a NOVA multi-gas analyzer and a California Analytical Instruments (CAI) CO_2 analyzer. Independent measurements were performed to characterize the dead volume of the system [27]. Subsequently, breakthrough experiments were corrected for dead volume and the corrected responses were used to determine the equilibrium loading capacity of CO_2 at the conditions explored in the experiments. The adsorption equilibrium data has been recently reported elsewhere [28]. Examples of the breakthrough curves from the CAI CO_2 analyzer are shown in the supporting information (Fig. S3).

Several isotherm models were considered to describe the equilibrium data from the breakthrough experiments. The Sips isotherm model, given by Eq. 1, was selected since it provided a good fit at the conditions explored. The Sips isotherm model for describing adsorption equilibria of CO_2 and H_2 on activated carbons can also be found elsewhere in the literature [9,23]. The solid phase loading, q_i^*, which is the solid phase concentration of the adsorbate which is in equilibrium with its fluid phase concentration, is given as

$$q_i^* = \frac{q_{\text{sat},i}(k_i p_i)^{s_i}}{1 + (k_i p_i)^{s_i}} \tag{1}$$

where $q_{\text{sat},i}$ is the temperature dependent saturation solid phase concentration, k_i is the adsorption equilibrium constant, s_i is a parameter which describes the homogeneity of the surface, and p_i is the partial pressure of component i. The parameter s_i can take values between 0 and 1. As the parameter s_i approaches unity, the Sips isotherm model takes the form of a simple Langmuir isotherm model. The quantities $q_{\text{sat},i}$, k_i and p_i are defined as follows

$$q_{\text{sat},i} = \omega_i e^{-\frac{\varphi_i}{RT}} \tag{2}$$

$$k_i = \theta_i e^{-\frac{\phi_i}{RT}} \tag{3}$$

$$s_i = s_{1,i}\arctan(s_{2,i}(T - T_{\text{ref}})) + s_{\text{ref},i} \tag{4}$$

The Sips isotherm model contains eight parameters ω_i, ψ_i, θ_i, ϕ_i, $s_{1,i}$, $s_{2,i}$, T_{ref} and $s_{\text{ref},i}$ that were fitted by performing a nonlinear regression using the experimental dynamic column breakthrough experiments. The parameters obtained for CO_2 are as follows: $\omega_{CO_2} = 3.74$ mol kg^{-1}; $\varphi_{CO_2} = -7.87$ kJ mol^{-1}; $\theta_{CO_2} = 26.9 \times 10^{-9}$ Pa^{-1}; $\phi_{CO_2} = -2.05$ kJ mol^{-1}; $s_{1,CO_2} = 0.136$; $s_{2,CO_2} = 0.110$; $s_{\text{ref},CO_2} = 0.760$ and; $T_{\text{ref},CO_2} = 281$ K. The fitted isotherm and the experimental data at 180°C, 240°C, and 300°C for CO_2 is illustrated in Fig. 2. Hydrogen isotherms were not available on TDA AMS-19. Hence, Sips isotherm parameters for H_2 on activated carbon available in the literature were used for cycle design and optimization studies presented in this work [22,23]. The H_2 parameters used are: $\omega_{H_2} = 6.66$ mol kg^{-1}; $\varphi_{H_2} = 0.0$ kJ mol^{-1}; $\theta_{H_2} = 0.7 \times 10^{-9}$Pa^{-1}; $\phi_{H_2} = -9.83$ kJ mol^{-1}; $s_{1,H_2} = 0$; $s_{2,H_2} = 0$; $s_{\text{ref},H_2} = 0.956$ and; $T_{\text{ref},H_2} = 273$ K. The heat of adsorption (ΔH_{ads}) for CO_2 on TDA AMS-19 was measured using differential scanning calorimetry and was found to be 20.5 kJ mol^{-1}. Since multi-component experimental data were not available for the adsorbent, single component isotherm parameters wereretained and it was assumed that they can reliably predict multi-component behavior for the given conditions using the extended Sips isotherm model given by the following equation

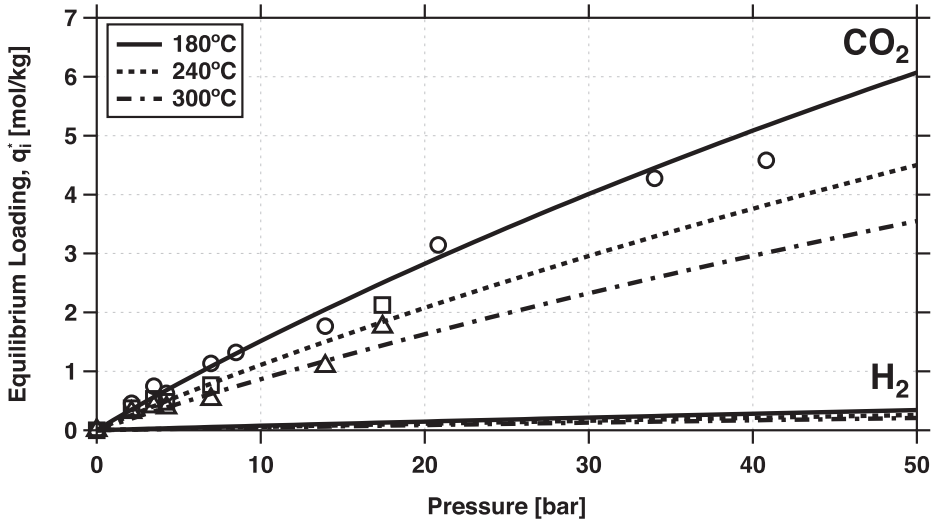

Fig. 2. Single component Sips isotherms for CO_2 and H_2. The CO_2 isotherm was measured at 180 (circles), 240 (squares) and 300 °C (triangles) at TDA Research Inc. while H_2 data for activated carbon was obtained from the literature [22]. Symbols are experimental values and the solid lines are the Sips isotherm fits. Each breakthrough experiment, from which the loadings were calculated, was repeated three times. The calculated loadings from these experiments were within 1% of the values reported in the plot.

$$q_i^* = \frac{q_{\text{sat},i}(k_i p_i)^{s_i}}{1 + \sum_{i=1}^{n_{\text{comp}}}(k_i p_i)^{s_i}} \quad (5)$$

where n_{comp} is the total number of components in the multi-component system.

3. Modeling

The adsorption column dynamics were simulated using a non-isothermal, non-isobaric detailed one-dimensional model described in Haghpanah et al. [29]. The model equations, listed in the supporting information, were obtained based on the following assumptions:

- An axially dispersed plug flow model describes the gas flow through the packed bed column
- The gas phase follows ideal gas behavior similar to other studies in the literature [9,10,29]
- The mass transfer resistance can be described using the linear driving force (LDF) model
- There are no concentration, temperature or pressure gradients in the radial direction
- Darcy's law can describe the pressure drop along the column in the axial direction
- Heat is transferred through the column wall
- The adsorbent properties and bed voidage remain uniform along the column
- The gas and solid phases reach thermal equilibrium instantaneously

The model equations were extended to simulate the pressure swing adsorption cycles by choosing appropriate initial and boundary conditions. The cycle steps studied in this work were categorized into three types: open-open, open-closed, and closed-open. The corresponding boundary conditions are given in the supporting information. For all simulations, the bed was initially saturated with H_2 at the feed conditions. The partial differential equations (PDEs) were discretized in the axial direction into 30 volume elements using a finite-volume technique with a van-Leer flux limiter, similar to that described in Haghpanah et al. [29–31]. The resulting system of ordinary differential equations (ODEs) were solved in MATLAB using a stiff solver, *ode23s*. Cyclic steady state (CSS) was considered to be achieved when a mass balance error for each component equals to or less than 0.5% for five consecutive cycles.

All simulations were performed with a unibed approach, i.e., a single bed was used to perform all the constitutive steps of given cycle in a specified sequence. For cycles involving coupled steps, the output stream data was stored in data buffers and then were used as input stream data for the other coupled steps. The model predicted the dynamics of the column and also provided detailed gas phase, solid phase and temperature profiles across the column. The model used in this work has been validated for a variety of separations including post-combustion CO_2 capture, air-separation at both lab- and pilot-scales [32–34]. It has been shown that both transient profiles and process performance indicators such as purity/recovery and energy can be reliably predicted by the model which takes input from characterization experiments such as the one described in this work.

4. Optimization framework

The framework used, also described in our previous studies, deals with solving two optimization problems [29,35–38]. The first involves the unconstrained simultaneous maximization of CO_2 purity and recovery. The purpose of solving this optimization problem was to identify the PSA cycles that meet the US-DOE requirements of 95% CO_2 purity and 90% recovery, respectively [39]. The second optimization problem was formulated to simultaneously minimize the energy consumption for CO_2 capture and maximize the productivity subject to the constraints of CO_2 purity and recovery. The PSA cycles that meet the CO_2 purity and recovery targets were considered for the second optimization problem. The objectives considered for the optimization problems, calculated at CSS, were defined as:

$$\text{CO}_2\text{ Purity, } Pu_{\text{CO}_2}[\%] = \frac{\text{Total moles of CO}_2\text{ in extract product in one cycle}}{\text{Total moles of gas in extract product in one cycle}} \times 100 \quad (6)$$

$$\text{CO}_2\text{ Recovery, } Re_{\text{CO}_2}[\%] = \frac{\text{Total moles of CO}_2\text{ in extract product in one cycle}}{\text{Total moles of CO}_2\text{ fed into the column in one cycle}} \times 100 \quad (7)$$

$$\text{Energy, } En\left[\frac{\text{kWh}_e}{\text{tonne CO}_2\text{ captured}}\right] = \frac{E_c + E_s + E_h}{\text{Mass of CO}_2\text{ in the extract product}} \quad (8)$$

$$\text{Productivity, } Pr\left[\frac{\text{mol. CO}_2}{m^3\text{ adsorbent. s}}\right] = \frac{\text{Total moles of CO}_2\text{ in the extract product}}{(\text{Total volume of adsorbent})(\text{Total cycle time})} \quad (9)$$

where E_c is the energy required to compress the product CO_2 stream to 150 bar; E_s is the energy lost from the use of steam; and E_h is the additional compression energy required to compress the H_2 stream to feed pressure. It is worth noting that the total cycle time in Eq. (9) refers to the sum of the constituent step times. During the scale up process, the introduction of idle times in order to synchronize the steps and to ensure that feed can be introduced in a continuous manner might be required. This increases the total cycle time and reduces the eventual productivity. Hence, the value of *Pr* calculated according to Eq. 9 represents an approximate estimate.

The European Benchmarking Task Force recommendations were used as guideline to describe the CO_2 compression [40]. The CO_2 compression energy was modeled as a multistage compression with inter-stage cooling to 25 °C. The critical pressure of CO_2 (P_c) is ≈ 73.8 bar [41], therefore, multistage compressors were used up to 73.8 bar and beyond 73.8 bar, a pump was used to deliver the CO_2 to 150 bar, as shown below:

$$E_c = N\frac{1}{\eta_c} n_{\text{in}} R T_{\text{in}} \frac{\gamma}{\gamma - 1}\left[\left(\frac{P_{\text{out}}}{P_{\text{in}}}\right)^{\frac{\gamma-1}{\gamma}} - 1\right] + \frac{W_{\text{pump}}}{\eta_{\text{pump}}} \quad (10)$$

where N is the number of stages; η_c = 80% is the compressor efficiency [42]; W_{pump} is the ideal work done by the pump and η_{pump} = 75% is the overall pump efficiency [40]. It was also assumed that in each stage compression, a maximum pressure ratio of 3 can be attained [42]. The heat that could be recovered in the intercoolers was not considered. The work done by the pump (W_{pump}) was calculated using the mechanical energy balance.

The PSA cycles proposed in this work require steam to purge the column for regeneration. It is assumed that the steam consumption required in the PSA cycles is independent of the steam generated in an IGCC power plant. The electrical energy corresponding to the steam consumption modeled based on the difference in steam enthalpy is shown below:

$$E_s = \eta_s m_{\text{steam}}(H_s - H_{\text{out}}) \quad (11)$$

where H_s is the enthalpy of steam at the operating pressure (P_L) and temperature (T_{pur}) of the purge step; H_{out} = 1978.9 kJ kg^{-1} is the enthalpy of steam that would typically be found in the exit stream of steam turbine [5]; and η_s = 88% was the steam turbine efficiency [40]. The enthalpy of steam, H_s, was calculated using the empirical equations available in the literature [43,44]. The saturation temperature of the steam based on the pressure P_L was calculated using:

$$\frac{T_{sat}}{T_c} = \frac{\left\{\sum_{i=0}^{2} a_i \left[\ln\frac{P_L}{P_c}\right]^i\right\}}{\left\{\sum_{j=0}^{5} A_j \left[\ln\frac{P_L}{P_c}\right]^j\right\}} \quad (12)$$

where $T_c = 647.096$ K and $P_c = 220.64$ bar are the steam critical temperature and pressure, respectively. The coefficients used in Eq. 12 are given in Table S2. Based on the saturation temperature, T_{sat}, the specific enthalpy of saturated steam (h_s) was calculated as follows:

$$\ln h_s = \sqrt{\chi_1 + \chi_2\left[\ln\frac{1}{T_r}\right]^{0.35} + \chi_3\frac{1}{T_r^2} + \chi_4\frac{1}{T_r^3} + \chi_5\frac{1}{T_r^4}} \quad (13)$$

where reduced temperature, $T_r = \frac{T_{sat}}{T_c}$. The coefficients are given in Table S3. It was also ensured that no steam condensation occurs in the column by super-heating the steam to 30°C above the saturation conditions. Based on the temperature of the PSA column, T_{PUR}, the steam temperature (T_{steam}) was calculated as:

$$T_{steam} = \begin{cases} T_{PUR}, & \text{if } T_{sat} + 30\ ^\circ\text{C} < T_{PUR} \\ T_{sat} + 30\ ^\circ\text{C}, & \text{otherwise} \end{cases} \quad (14)$$

Typically, a temperature gradient would exist across the column at the beginning of the purge step. Hence, as a cautionary measure, T_{PUR} is considered as the maximum temperature within the column. The specific enthalpy (H_s) of steam used in the PSA process can be written as,

$$H_s = h_s + \Delta h_s \quad (15)$$

where, $\Delta h_s = C_{p,steam}(T_{steam} - T_{sat})$, represents the specific enthalpy required to super-heat the steam.

The performance of pre-combustion CO_2 capture process is evaluated based on two key performance indicators, namely energy consumption and productivity while guaranteeing a certain minimum product purity and recovery. These type of problems fall into the category of constrained multi-objective optimization problems. There are several optimization techniques to solve such problems. In this work Genetic Algorithm (GA), a technique that mimics evolutionary processes, is employed [45]. The technique starts with an initial "population" that consists of a collection of unique set of decision variables. The GA passes these individuals to the PSA model which evaluates their fitness with respect to the specified objective function(s). At the end of a "generation", the fitness of the individuals is used as a criteria to select the next generation. During this process, operators such as mutation, crossover, etc., are used to improve the diversity of the population. This process is repeated for several generations until there can be no more improvement in the fitness of the individuals. Genetic algorithms have been extensively used for optimizing a variety of chemical processes and enjoy the success as they are generally good at escaping local minima, a shortcoming that is faced by gradient-based optimization approaches.

The multi-objective optimization problems were solved using a non-dominated sorting genetic algorithm (NSGA-II) in MATLAB global optimization toolbox [45]. Previous studies have shown that NSGA-II can be easily coupled with the detailed PSA model and parallelized for rapid optimizations [29]. The computations were performed on a desktop workstation with two 12-core INTEL Xeon 2.5 GHz processors and 128 GB RAM. A multidimensional search space was defined for the optimizer, based on the decision variables (DVs), which were the cycle step times (t_{ADS}, t_{CoBLO}, t_{CnBLO}, t_{PREQ}, t_{PUR}, etc.), low pressure (P_L), intermediate pressure (P_I,), feed velocity (v_0) and purge velocity (v_{PUR}).

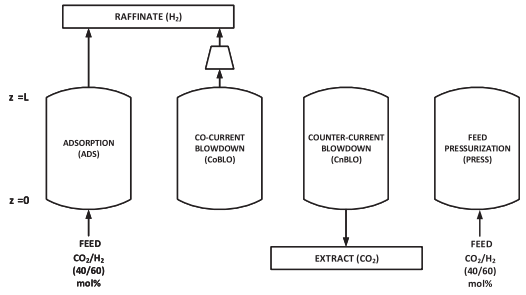

A. Basic 4-step PSA cycle

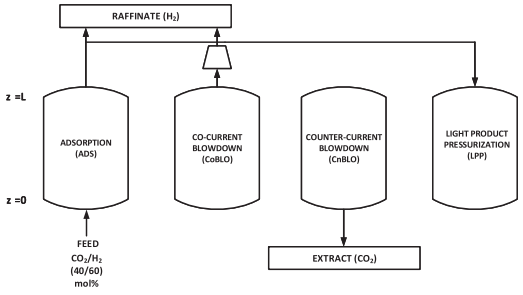

B. 4-step PSA cycle with LPP

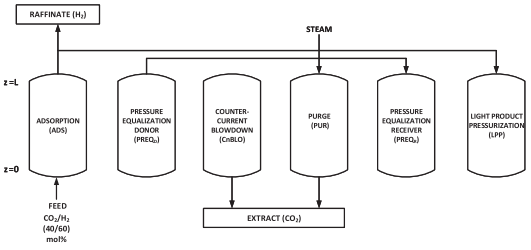

C. 6-step PSA cycle with CnBLO, purge, PREQ & LPP

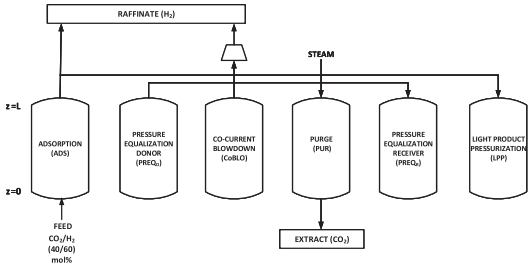

D. 6-step PSA cycle with CoBLO, purge, PREQ & LPP

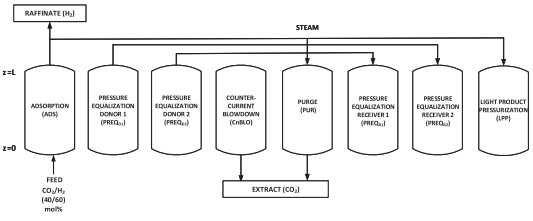

E. 8-step PSA cycle with CnBLO, purge, two PREQ & LPP

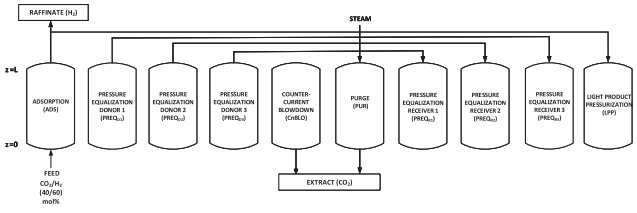

F. 10-step PSA cycle with CnBLO, purge, three PREQ & LPP

Fig. 3. PSA cycle configurations considered in this study.

The LPP step time (t_{LPP}) was obtained based on the time required by the column to reach the high pressure (P_H), which was dependent on the exit flow rate of the adsorption step. The high pressure (P_H) was kept constant at 34.5 bar. An initial population for GA was generated using Latin-Hypercube (LHC) sampling, a sampling technique based on probability distribution. The population size of 24 times the number of decision variables were used. In this work, the GA was run for 50 generations.

5. Cycle design & simulation

A variety of PSA cycles were designed and the performance indicators, viz. purity and recovery, were used to evaluate the proposed cycles after performing full cycle simulations to CSS. All cycle configurations are shown in Fig. 3. The parameters and process conditions used for the simulations are provided in Tables 1 and 2. A feed velocity of 0.1 m s^{-1}; a purge velocity of 0.3 m s^{-1} and; a low pressure of 10 bar were used for these simulations. The description of each cycle configuration is discussed below.

5.1. Configuration A: basic 4-step PSA cycle

This cycle configuration consists of a feed pressurization, adsorption (ADS), co-current blowdown (CoBLO) and counter-current blowdown (CnBLO) steps. The feed, a mixture of 40 mol% CO_2 and 60 mol% H_2, enters the column at the feed end ($z = 0$) in the adsorption step. At the light product end ($z = L$), weakly adsorbing H_2 is collected, while the strongly adsorbed CO_2 remains in the column. The adsorption step is followed by a co-current blowdown where the residual H_2 present in the column is further removed at the light product end. To regenerate the column, CO_2 is extracted out of the feed end in the counter-current blowdown step. This is followed by a feed pressurization to bring the column back to the feed pressure.

In this cycle, CO_2 is collected in the counter-current blowdown step while the H_2 product is obtained from the adsorption and the co-current blowdown steps. The H_2 product obtained from the co-current blowdown step at an intermediate pressure requires a compressor to raise the pressure of the raffinate stream from an intermediate pressure to high pressure for further processing. At the conditions provided in Table 2, the basic 4-step cycle simulation resulted in a CO_2 purity and recovery of 70% and 33%, respectively (shown in Table 2). For these conditions, it was found that CO_2 was lost both in the adsorption and co-current blowdown steps which were primarily raffinate product steps. This can be confirmed from Fig. S4 (provided in the supporting information), which shows the cumulative CO_2 collected at the end of each step. These observations led to a modification in the cycle configuration to reduce the CO_2 losses from the adsorption and the co-current blowdown steps.

5.2. Configuration B: 4-step PSA cycle with light product pressurization

In this cycle configuration, the feed pressurization step in configuration A was replaced with a light product pressurization (LPP). In the LPP step, a part of the raffinate product from the adsorption step is sent back to the column for pressurization. This step improves the CO_2 recovery, since the CO_2 leaving in the light product stream in the adsorption step is returned to the column. However, a LPP step reduces the H_2 recovery, since part of the H_2 is fed back into the column. The feed conditions of the LPP step were the outlet conditions of the adsorption step. This was modeled using a data buffer that saves the profiles at the exit of the adsorption step. If the desired pressure is not achieved by LPP alone, a feed pressurization is also performed.

A full cycle simulation was performed for this modified configuration. As expected, the CO_2 losses from the adsorption step were reduced when compared to configuration A (as shown in Fig. S4) and the cycle increased CO_2 recovery. However, this also led to a slightly lower H_2 recovery since part of the H_2 product was used to pressurize the column. The addition of the LPP step pushes the CO_2 front towards the $z = 0$ end, reducing CO_2 losses in the subsequent steps. The conditions (listed in Table 2) chosen for this configuration were same as the basic 4-step cycle conditions. Although, there was an improvement in the CO_2 recovery, the major short-coming of this cycle would be the incomplete regeneration of the bed for the adsorption step.

5.3. Configuration C: 6-step PSA cycle with counter-current blowdown, purge, pressure equalization and light product pressurization

The previous cycle configuration was modified to a 6-step PSA cycle by adding a purge (PUR) and pressure equalization (PREQ) steps. A purge step was introduced to remove any residual CO_2 remaining in the column to further regenerate the column. Steam at pressure P_L was used to regenerate the column as it was assumed that steam does not adsorb on TDA AMS-19 and can be separated from the product stream through compression and cooling. A purge step further extracts the CO_2 from the column after a counter-current blowdown step, increasing the recovery of CO_2. The outlet stream of the purge step is a wet stream. The CO_2 and H_2 purity reported in this work were on dry basis. A pressure equalization step consists of a donor column and a receiver column. In the donor step, depressurization from P_H to P_I occurs, similar to a co-current blowdown step. The exit stream of this step was used to pressurize the receiver column. Another advantage of replacing the co-current blowdown step with a pressure equalization is that the light product H_2 is collected only at pressure P_H in the adsorption step, therefore, avoiding an additional compression step to deliver H_2 at a high pressure P_H. The intermediate pressure P_I cannot be arbitrarily fixed and depends on P_H and P_L in the cycle. The P_I was estimated using an empirical correlation that was obtained by running a local optimization to minimize the difference between the moles leaving the donor step and

Table 1
PSA simulation parameters.

Parameter	Value	Source
Column Properties		
Length, L [m]	0.83	Measured
Outer radius, $r_o[m]$	5.715×10^{-2}	Measured
Inner radius, $r_i[m]$	5.118×10^{-2}	Measured
Particle radius, r_p [m]	3×10^{-4}	Measured
Bed voidage, ϵ [–]	0.4	Assumed
Particle voidage, ϵ_p [–]	0.57	Measured
Physical Properties		
Adsorbent density, ρ_s [kg m^{-3}]	1361.00	Measured
Specific heat capacity of adsorbent, $C_{p,s}$ [J kg^{-1} K^{-1}]	1877.20	Assumed
Specific heat capacity of gas phase, $C_{p,g}$ [J kg^{-1} K^{-1}]	1010.60	NIST database
Molecular diffusivity, D_m [m^2 s^{-1}]	4.81×10^{-8}	Calculated
Fluid viscosity, μ [kg m^{-1} s^{-1}]	2.15×10^{-5}	Standard value
Effective gas thermal conductivity, K_z [J m^{-1} K^{-1} s^{-1}]	0.09	Fitted
Inside heat transfer coefficient, h_{in} [J m^{-2} K^{-1} s^{-1}]	0	Assumed
Outside heat transfer coefficient, h_{out} [J m^{-2} K^{-1} s^{-1}]	2.5	Assumed
Universal gas constant, R [m^3 Pa mol^{-1} K^{-1}]	8.314	Standard value
Mass transfer coefficient, CO_2, k_{avg,CO_2} [s^{-1}]	0.53	Calculated
Mass transfer coefficient, H_2, k_{avg,H_2} [s^{-1}]	10	Calculated
Heat of adsorption CO_2, ΔH_{CO_2} [kJ mol^{-1}]	20.5	Measured
Heat of adsorption H_2, ΔH_{H_2} [kJ mol^{-1}]	9.8	Literature [23]
Operating parameters		
Syngas feed pressure P_{feed} [bar]	34.5	IGCC conditions
High pressure P_H [bar]	34.5	IGCC conditions
Feed composition (CO_2/H_2), y_{feed} [–]	0.4/0.6	IGCC conditions
Feed temperature, T_{feed} [°C]	240	IGCC conditions

Table 2
Summary of PSA cycle simulations. For configurations A & B, P_{CoBLO} was represented as P_{I1}. * indicates that intermediate pressures for pressure equalization steps were calculated based on P_H & P_L and were not fixed in the simulations. For the cycles involving steam purge, the purities are reported on a dry basis.

Cycle configuration	t_{ADS} [s]	t_{CoBLO} [s]	t_{CnBLO} [s]	t_{PRESS} [s]	t_{PUR} [s]	t_{PREQ1} [s]	t_{PREQ2} [s]	t_{PREQ3} [s]	P_{I1} [bar]	P_{I2} [bar]	P_{I3} [bar]	P_L [bar]	CO_2		H_2	
													Purity [%]	Recovery [%]	Purity [%]	Recovery [%]
A	40	45	95	20	–	–	–	–	21.8	–	–	10	70.1	33.2	67.0	90.6
B	40	45	95	t_{LPP}	–	–	–	–	21.8	–	–	10	70.9	44.7	70.4	87.8
C	40	–	95	t_{LPP}	20	45	–	–	21.8*	–	–	10	75.2	99.9	99.9	77.7
D	40	95	–	t_{LPP}	20	45	–	–	21.8*	–	–	10	93.3	99.3	99.6	95.1
E	40	–	95	t_{LPP}	20	15	30	–	25.5*	17.5*	–	10	80.5	99.9	99.9	83.6
F	40	–	95	t_{LPP}	20	15	15	15	27.4*	21.4*	15.6*	10	83.5	99.9	99.9	86.3

that entering the receiver column [37].

The modifications in the cycle improved the performance metrics when compared to the two cycles discussed in the previous subsections. The fluid and solid phase profiles are shown in the supporting information (Figs. S5 and S6). The CO_2 purity increased marginally to 75%. The addition of a purge step in the process increased the CO_2 recovery by removing the remaining CO_2 from the solid phase at the end of the purge step. The raffinate product end ($z = L$) of the column (as shown in Fig. S6(a) of the supporting information) was not contaminated by the extract product (CO_2), and CO_2 was not lost in the raffinate product step (ADS in Fig. S6(a)); the purge step led to pure H_2 being obtained. After the purge step, CO_2 and H_2 were present in trace amounts in both the solid and the gas phases. The weakly adsorbing steam was present in the gas phase and the column was saturated with steam at the end of purge step (PUR in Fig. S6(b) of the supporting information). The steam which remained in the gas phase was removed during the adsorption step and after the removal of the steam, pure H_2 product was obtained. The addition of the purge step further regenerated the bed and the working capacity of CO_2 improved when compared to the cycles discussed before. However, configuration C provided a lower H_2 recovery when compared to the previous two cycles.

5.4. Configuration D: 6-step PSA cycle with co-current blowdown, purge, pressure equalization and light product pressurization

Configuration C was modified by replacing the counter-current blowdown step with a co-current blowdown step. The co-current blowdown step will remove the H_2 gas present in the column after the pressure equalization donor step. In the co-current blowdown step, the column is depressurized from P_I to P_L. Since the H_2 gas is pulled out from the raffinate product end ($z = L$), the residual H_2 present in the column, during the co-current blowdown step, moves towards the raffinate product end. In the subsequent steam purge step, pure CO_2 is extracted from the column. This configuration increases the CO_2 purity and also the H_2 recovery. The H_2 gas collected in the co-current blowdown step is at a lower pressure than the H_2 gas obtained in the adsorption step and hence, must be compressed to P_H in an additional processing step.

Fig. 4 shows H_2 solid phase profiles for cycle configurations C & D, respectively. Reversal of the counter-current blowdown step into a co-current blowdown step removed the H_2 which remained in the bed at the end of the pressure equalization step (donor column). H_2 was removed from the raffinate product end ($z = L$) and at the end of the co-current blowdown step, H_2 front moved to the raffinate product end and the extract product end ($z = 0$) was rich in CO_2. This led to pure CO_2 being obtained during the purge step which was the CO_2 product step in the new configuration and it was reflected by the comparatively higher CO_2 purities (93%). This can be best explained by considering the H_2 solid phase profiles and the amount of H_2 being removed in the CO_2 product steps, which is given by the shaded region in Fig. 4. For configuration C, the cycle with counter-current blowdown, the amount of H_2 present in the CO_2 product stream (shown as dashed and dotted area in Fig. 4) was higher than the amount of H_2 in the CO_2 product stream in the reversed counter-current blowdown PSA cycle (dotted in Fig. 4).

5.5. Configurations E & F: Addition of pressure equalization steps to configuration C

In configuration E, an additional pressure equalization step was added to configuration C. The extra pressure equalization increases the CO_2 purity by removing more H_2 from pressure equalization donor steps. The first donor column is depressurized from P_H to P_{I1}, while the second donor column is depressurized from P_{I1} to P_{I2}. The receiver columns are pressurized from P_L to P_{I1} and P_{I1} to P_{I2} using the desorbed gas from the two donor steps. The intermediate pressures for the

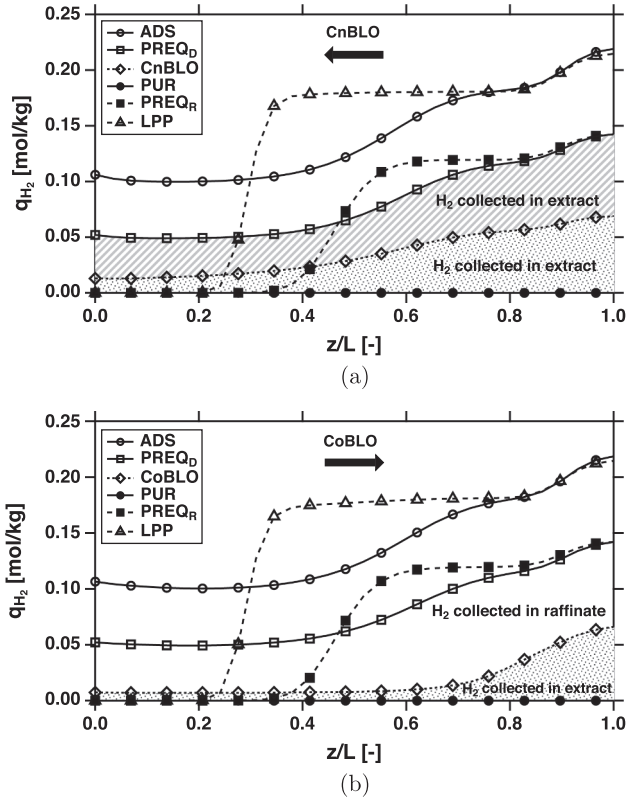

Fig. 4. H_2 solid phase profiles at the end of each step for (a) Configuration C and (b) Configuration D for operating conditions reported in Table 2. The shaded area represents the H_2 collected in the extract stream and the arrows represent the direction of the blowdown step.

pressure equalization steps were determined using empirical correlations. These empirical equations were formulated by performing a local optimization to minimize the difference between the moles of gas leaving the donor step and moles of gas entering the receiver step for the two pressure equalization steps. In configuration F, two additional pressure equalization steps were added to configuration C. Similar to previous configurations, the intermediate pressures P_{I1}, P_{I2} and P_{I3} for the pressure equalization steps were determined using empirical correlations.

As it can be seen from Table 2, the addition of pressure equalization steps (configuration E and F) improved the CO_2 purity when compared to configuration C with one pressure equalization. The two (configuration E) and three (configuration F) pressure equalizations helped in removing more H_2 in the pressure equalization steps by reducing the intermediate pressures to 17.5 bar and 15.6 bar, respectively, while for the configuration C the intermediate pressure at the end of pressure equalization was 21.8 bar. The lower intermediate pressures in configuration E and F led to the removal of more H_2 while enriching CO_2 at the extract product end. The solid phase profiles for H_2 for all three configurations are shown in Fig. 5. The amount of H_2 desorbed in the three cycles during the pressure equalization steps, given by the shaded region confirmed that the H_2 desorbed in the pressure equalization steps for the configuration F (donor column) was more as compared to the configuration E and significantly higher when compared to the configuration C. Identical process conditions for configurations C, E and F resulted in CO_2 purities of 75.2 %, 80.5% and 83.5%, respectively.

6. Process optimization: maximization of purity and recovery

A detailed multi-objective optimization was performed to maximize the CO_2 purity and recovery, simultaneously, for all cycle configurations. Regulatory bodies such as the US-DOE have imposed CO_2 purity and recovery requirements of 95% and 90%, respectively [39]. The PSA cycles considered were subjected to the maximization of CO_2 purity-recovery in order to identify the operating conditions that would satisfy these targets. The lower and upper bounds of the decision variables are provided in Table 3. The optimizer generates a Pareto curve, which is the best trade-off between the CO_2 purity and recovery for a given cycle configuration. The region above Pareto curve is considered to be infeasible for that cycle configuration. The objectives for optimization problem were defined as follows:

$$\min J_1 = \frac{1}{Pu_{CO_2}} \tag{16a}$$

$$\min J_2 = \frac{1}{Re_{CO_2}} \tag{16b}$$

Fig. 6 shows the Pareto curves for all the six PSA cycle

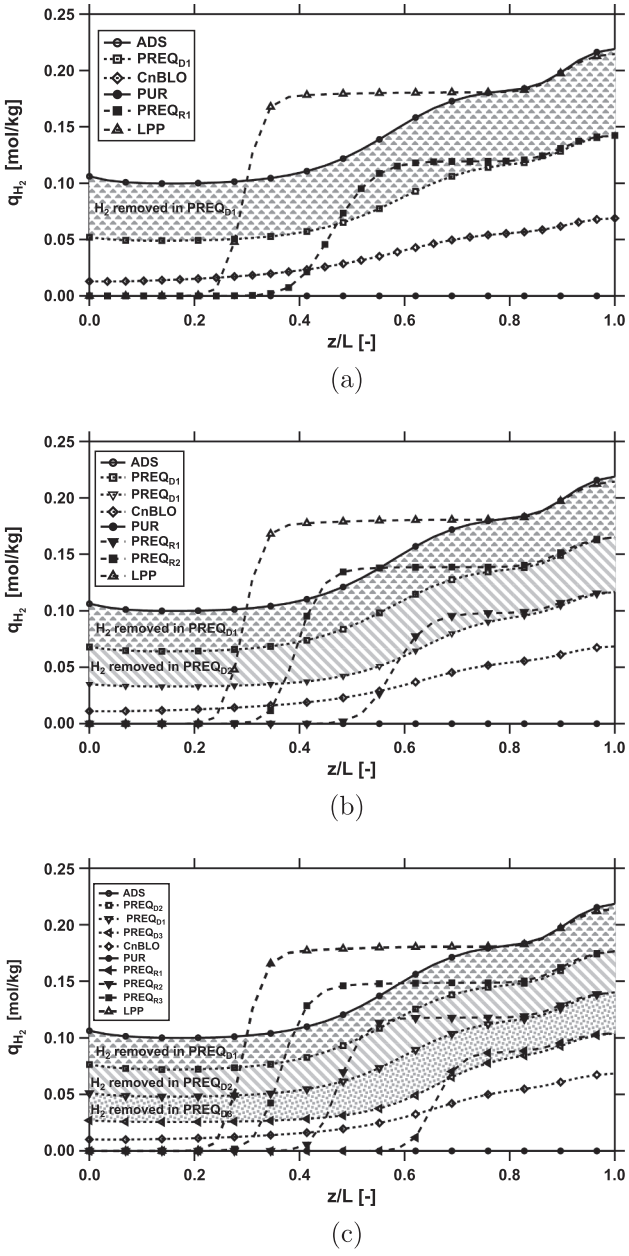

Fig. 5. H_2 solid phase profiles at the end of each step for (a) Configuration C, (b) Configuration E and (c) Configuration F corresponding to the operating conditions provided in Table 2. The shaded area represents H_2 collected in pressure equalization step(s).

Table 3
Bounds for decision variables provided to the optimizer.

Configuration	t_{ADS} [s]	t_{CoBLO} [s]	t_{PREQ1} [s]	t_{PREQ2} [s]	t_{PREQ3} [s]	t_{CnBLO} [s]	t_{PUR} [s]	P_I [bar]	P_L [bar]	v_0 [m s^{-1}]	v_{PUR} [m s^{-1}]
A	20–100	30–200	–	–	–	30–200	–	17.3–34.5	1–17.3	0.08–0.8	–
B	20–100	30–200	–	–	–	30–200	–	17.3–34.5	1–17.3	0.08–0.8	–
C	20–100	–	30–200	–	–	30–200	10–80	–	1–17.3	0.08–0.8	0.1–1
D	20–100	30–200	30–200	–	–	–	10–80	–	1–17.3	0.08–0.8	0.1–1
E	20–100	–	30–200	30–200	–	30–200	10–80	–	1–17.3	0.08–0.8	0.1–1
F	20–100	–	30–200	30–200	30–200	30–200	10–80	–	1–17.3	0.08–0.8	0.1–1

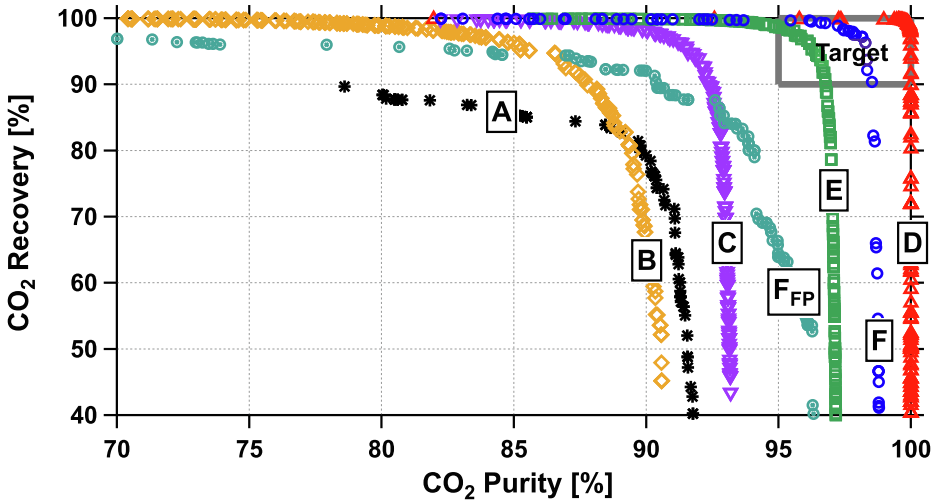

Fig. 6. CO_2 purity-recovery Pareto fronts for six different PSA cycles. F_{FP} corresponds to a variant of configuration F with feed purge instead of steam.

configurations considered in this study. The purities are reported on dry basis. The basic 4-step cycle (configuration A) had optimum purity-recovery points less than 90%. Therefore, the cycle configuration is not suitable for use. The CO_2 recoveries are much lower than the other cycle configurations. The CO_2 losses come from the adsorption or co-current blowdown steps. Modifying the feed pressurization to LPP in configuration B has significantly improved the CO_2 recoveries, however, the CO_2 purity drops because the portion of H_2 stream exiting the adsorption step is sent back to column. Although, configuration B meets the CO_2 recovery targets, it falls short of purity constraints. The addition of a pressure equalization step in configuration C has improved the CO_2 purity. Configuration C has a Pareto front which is in the far top-right when compared to configuration A. The maximum purity that can be achieved using this configuration is limited to 92%. The introduction of pressure equalization step significantly improved the CO_2 recoveries. This is because CO_2 was not lost in the raffinate product stream. The addition of a purge step also contributes to the increase in CO_2 recoveries because the CO_2 retained in the column after the counter-current blowdown step is pushed out of the column during the purge step. Reversing the counter-current blowdown to a co-current blowdown step in configuration D has greatly improved the CO_2 purity. This is because most of the H_2 is removed from the column in the co-current blowdown step and when the column is purged, pure CO_2 is obtained. Configuration D also satisfies the regulatory requirements of CO_2 purity-recovery for sequestration. In configuration E, addition of a pressure equalization improved the CO_2 purity. Since the H_2 is removed from the raffinate end of the column at two intermediate pressures, the exit stream in the counter-current blowdown and purge steps is enriched with CO_2, increasing the CO_2 purity. The optimization of configuration F with three pressure equalization steps further improved the CO_2 purities and pushed the Pareto front towards the target region. The key decision variables for the Pareto fronts reported in Fig. 6 are illustrated in Fig.S7 in the supporting information. It can be seen that the configurations were achieving the desired purities and recoveries at low feed velocities in order to prevent the breakthrough of CO_2 in the adsorption step. Also it is further shown in Fig.S7, the configuration D was able to achieve the targets at high values of P_L when compared to other configurations. This facilitates lower CO_2 compression energy consumption at the cost of increased H_2 compression.

Steam purge vs. feed purge

In order to investigate the effect of steam purge on CO_2 purity and recovery for the proposed PSA cycles, a case study was performed. For this analysis, two cases were considered for comparison. The first being configuration F that was originally proposed with steam purge. In the second case, the steam purge in Configuration F was replaced with the feed purge while keeping the rest of the steps the same. A maximization of CO_2 purity and recovery optimization was performed for the second case and the Pareto fronts are compared in Fig. 6. As it can be seen from the figure, the PSA cycle with feed purge underperforms the one with steam purge. The feed purge, while removing CO_2 from the solid phase, contaminates the column with H_2. The extra H_2 present in the column, due to the purge, exits the column along with CO_2 from the feed end of the column, reducing the CO_2 purity. Hence, the purpose of purging the column with feed to recover more CO_2 can be achieved only with low CO_2 purities, as shown in Fig. 6. The feed purge also reduces CO_2 recovery because the CO_2 that is present near the raffinate end of the column will be lost in the subsequent adsorption step. On the other hand, the advantage of having steam purge in the process improves the CO_2 recovery by removing the residual CO_2 present in the column for complete regeneration with no contamination. The weakly adsorbing steam which remains in the column can be removed during the adsorption step.

7. Process optimization: minimization of energy consumption and maximization of productivity

The purity-recovery Pareto fronts provide information on the ability on the cycles meeting the regulatory requirements. However, they do not provide any information regarding the energy and size of the process. The conversion of energy consumption and productivity in terms of cost is rather complex and beyond the scope of this work. For any separation process, it is desired to have least energy consumption and maximum productivity for the given constraints. Hence, minimizing the energy consumption and maximizing the productivity of CO_2 was considered for further evaluation of PSA cycles that has met the CO_2 purity-recovery targets. The objectives for this constrained multi-objective optimization was formulated as:

$$\min J_3 = \psi_1 En + \lambda_1 \left[\max\left(0, Pu_{\text{target}} - Pu_{CO_2}\right)\right]^2 + \lambda_2 \left[\max\left(0, Re_{\text{target}} - Re_{CO_2}\right)\right]^2 \quad (17a)$$

$$\min J_4 = \frac{\psi_2}{Pr} + \lambda_1 \left[\max\left(0, Pu_{\text{target}} - Pu_{CO_2}\right)\right]^2 + \lambda_2 \left[\max\left(0, Re_{\text{target}} - Re_{CO_2}\right)\right]^2 \quad (17b)$$

where ψ_1, ψ_2, λ_1 and λ_2 are penalty factors. $Pu_{\text{target}} = 95\%$ and $Re_{\text{target}} = 90\%$ were the purity and recovery targets that need to be achieved. The decision variables search space used for this optimization was same as the bounds used for purity-recovery optimizations.

As shown in the previous section, three PSA cycle configurations (D, E and F) met the CO_2 purity-recovery targets. For these cycles, minimization of energy consumption and maximization of productivity optimization was considered and the Pareto fronts are shown in Fig. 7(a). All the points in Fig. 7(a) correspond to different operating conditions for which the CO_2 purities and recoveries are greater than 95% and 90%, respectively. As it can been seen from the figure, the Pareto fronts of configurations E and F are quite close. It was found that configuration F (with 3 pressure equalization steps) achieved 95.0% and 90.8% CO_2 purity and recovery, respectively, with the least energy consumption of 95.7 kWh_e/tonne of CO_2 captured at a low productivity rate of 3.3 mol CO_2/m^3 adsorbent/s. The optimal step times corresponding to the minimum energy consumption are: t_{ADS} = 33.8 s, t_{PREQ1} = 39.5 s, t_{PREQ2} = 112.5 s, t_{PREQ3} = 77.7 s, t_{CnBLO} = 94.0 s, and t_{PUR} = 21.7 s; while, the operating conditions were P_L = 4.7 bar, v_0 = 0.2 m s^{-1}, and v_{PUR} = 0.2 m s^{-1}. For configuration E, the optimizer found the minimum energy consumption to be 105.4 kWh_e/tonne of CO_2 captured at a productivity rate of 3.5 mol CO_2/m^3 adsorbent/s for 95.5% and 90.3% CO_2 purity and recovery, respectively. The optimal decision variables corresponding to the minimum energy point are: t_{ADS} = 47.4

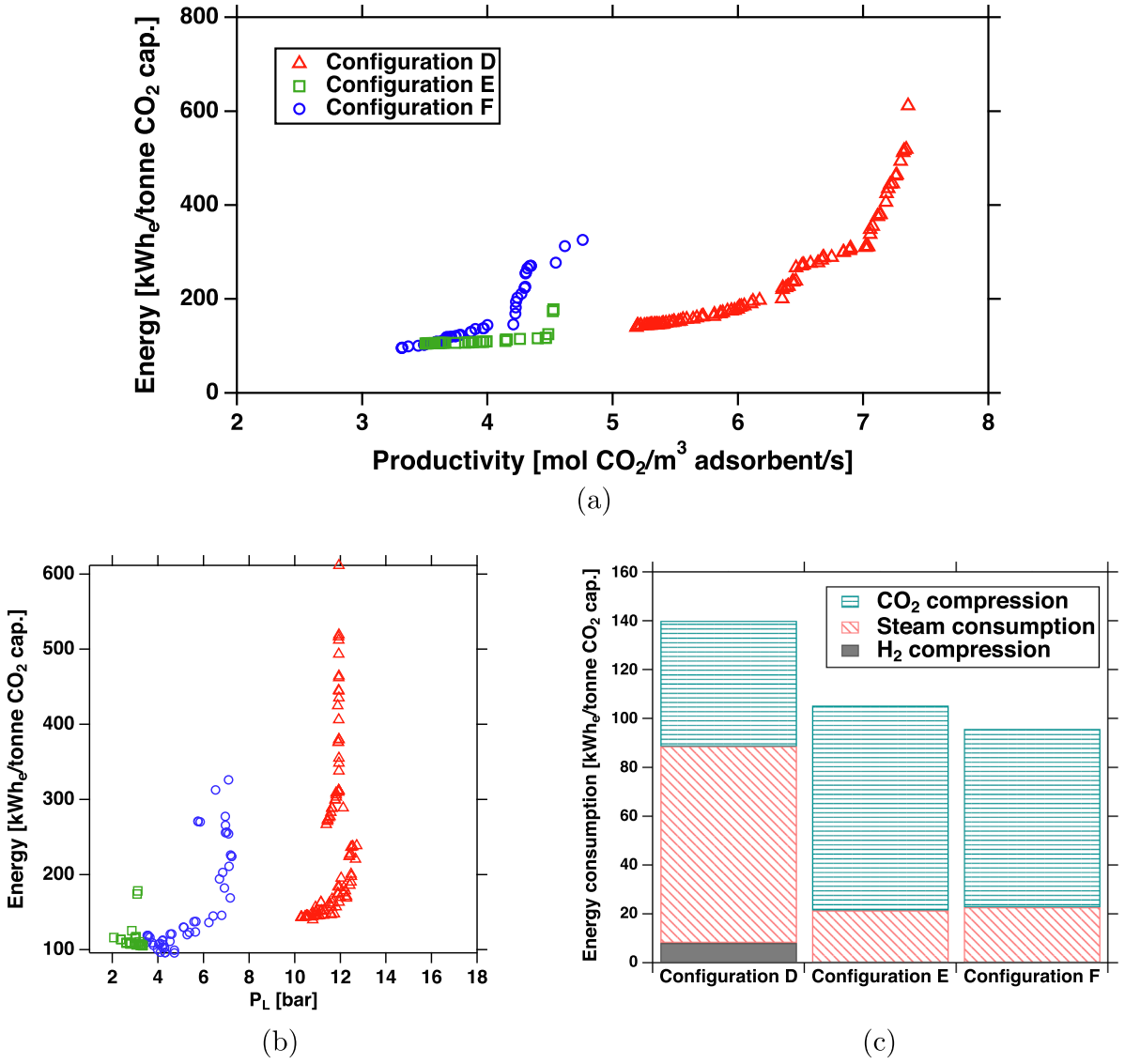

Fig. 7. (a) Energy-productivity Pareto fronts for configurations that met CO_2 purity-recovery requirements. (b) Low pressure (P_L) corresponding to the energy-productivity Pareto fronts of configuration D (triangles), configuration E (squares) and configuration F (circles) shown in (a). (c) Energy contributions from CO_2 compression, steam and H_2 compression corresponding to minimum energy consumption point for configurations D, E and F.

s, t_{PREQ1} = 122.0 s, t_{PREQ2} = 97.7 s, t_{CnBLO} = 105.5 s, and t_{PUR} = 41.7 s, P_L = 3.3 bar, v_0 = 0.1 m s^{-1}, and v_{PUR} = 0.1 m s^{-1}. It should be noted from Fig. 7(a), with increase in productivity, the energy consumption for configuration F goes higher than that of the configuration E (with 2 pressure equalization steps). It can be clearly seen from Fig. 7(b) that the low pressures (P_L) for configuration F are higher than that of configuration E, indicating that the residual CO_2 present in the column after the counter-current blowdown step is higher in case of configuration F as compared to configuration E and most of the CO_2 is recovered in the purge step. Hence, to achieve high productivities in case of configuration F, more steam is needed to completely sweep CO_2 out of the column, thus contributing to high energy requirements.

Another PSA cycle optimized for energy-productivity was configuration D. Configuration D has one pressure equalization step and a co-current blowdown step, instead of counter-current blowdown step as similar to other two configurations discussed above. The purpose of co-current blowdown step was to remove to more H_2 in the column so that in the subsequent purge step, CO_2 obtained will be of high purity. For this cycle configuration, the optimizer found the minimum energy consumption of 139.9 kWh_e/tonne of CO_2 captured for a productivity rate of 5.2 mol CO_2/m^3 adsorbent/s. The operating conditions corresponding to this performance are: t_{ADS} = 42.3 s, t_{PREQ1} = 108.9 s, t_{CnBLO} = 57.6 s, and t_{PUR} = 22.2 s, P_L = 10.8 bar, v_0 = 0.1 m s^{-1}, and v_{PUR} = 0.2 m s^{-1}. It is clear from Fig. 7(a) that the configurations E and F outperformed configuration D in terms of energy consumption while configuration D achieved higher productivities. This is because all of the CO_2 is recovered from only purge step unlike, other configurations which also has counter-current blowdown step to remove CO_2, thereby requiring more steam to purge the column in order to extract all the CO_2. Also, another energy penalty arises from compressing H_2 in the co-current blowdown step to feed pressure. It is also worth noting that for configuration D, the steam was required at high pressures (around 10–12 bar) when compared to configurations E and F, which needed steam at pressures 2–6 bar. Since, the enthalpy of steam is higher at higher pressures, the energy consumption arising from the steam purge step is quite substantial for configuration D. At this point, it is worth comparing the current results with those of Casas et al. [9], who studied a similar separation. In their work the focus was on maximizing purity and recovery. A 10-step cycle that has 4 pressure equalizations was able to achieve this target. Under these conditions, they reported a productivity of ≈ 17 mol CO_2/kg h (4.01 mol CO_2/m^3 s), which is comparable to the productivity values obtained in configurations E and F. The maximum productivity obtained in configuration D is 85% more than the productivity reported by Casas et al. This improved productivity clearly highlights the benefits of using a steam purge. Since configuration D involves just 1 pressure equalization, it is also possible that it requires fewer columns than those that would be needed to implement a cycle that has four pressure equalizations.

Fig. 7(c) shows the energy contribution from CO_2 compression, steam and H_2 compression corresponding to the respective minimum energy consumption for all the three configurations considered in the section. As discussed earlier, most of the energy penalty (≈ 80.5 kWh_e/tonne CO_2 for configuration D was from higher steam consumption at higher pressure as compared to configurations E and F, which were 21.4 kWh_e/tonne CO_2 and 22.8 kWh_e/tonne CO_2, respectively. The CO_2 compression was least for configuration D, which was 51.4 kWh_e/tonne CO_2. This was because the CO_2 was recovered at a higher pressure of 10.8 bar and compressed to 150 bar. On the other hand, for configurations E and F, CO_2 compression was done from ≈ 3–4 bar to 150 bar, thus consuming additional energy of 83.9 and 73.0 kWh_e/tonne CO_2, respectively. Configuration D also has an additional energy penalty for compressing H_2 from 10.8 bar to a feed pressure of 34.5 bar, while the other two configurations avoid this extra contribution.

The energy calculations performed in this study were based on the assumption that steam required in the process was obtained from an external source and not from IGCC power plant. Another key aspect was since H_2 isotherm data on TDA-AMS-19 was not available, isotherm parameters from the literature were used. To substantiate the validity of this assumption, a simple parametric analysis was performed to investigate how much would the minimum energy consumption reported for each of the three cycle configurations change when the H_2 equilibrium loadings change. To this end, the equilibrium loadings of H_2 were changed by ± 50% and simulations were performed for all the three cycle configurations for the operating conditions corresponding to the minimum energy consumption reported in Fig. 7(c). Figure S8 in the supporting information shows the effect of H_2 equilibrium loadings on the minimum energy consumption. When the equilibrium loadings were decreased by 50%, there was a negligible reduction in the energy. A maximum change of 3 % was noticed for configuration D. Therefore, H_2 isotherm did not have a significant impact on the energy consumption and the validity of the assumption still holds good. In a similar manner, a sensitivity analysis was performed on the CO_2 loadings, mass transfer coefficient and the heats of adsorption of CO_2 and H_2. Each of these parameters were varied by +10% and −10% and the simulations were repeated (see Table S4 in the supporting information for the details). The change of the key performance indicators, viz. purity, recovery, energy and productivity were calculated. The CO_2 isotherm and the mass transfer had an impact on the recovery and productivity values. A 10% change in these quantities resulted in a maximum of 6% variation in the recovery and productivity. However, the values of purity and the energy consumption were not affected much. The other parameters had a marginal effect on process performance.

8. Conclusion

Various PSA cycle configurations were evaluated for pre-combustion CO_2 capture using patented TDA AMS-19 adsorbent. The adsorption equilibria for CO_2 on TDA AMS-19 was experimentally measured and fitted to a Sips isotherm model. H_2 isotherm parameters for activated carbon were obtained from the literature. Six different PSA cycle configurations were designed and optimized for this study. A detailed one-dimensional PSA model, discretized using the finite volume method, was employed to describe the dynamics of the PSA cycles. The full-scale PSA simulations involved solving mass, momentum and energy balances so as to obtain the pressure, temperature and concentration profiles for gases. The performance indicators, namely, purity and recovery for CO_2 were calculated after the process reached the cyclic steady state. Firstly, an unconstrained multiobjective optimization was performed to maximize the CO_2 purity and recovery for six PSA cycle configurations in order to assess their ability to achieve regulatory requirements of CO_2 purity and recovery of 95% and 90%, respectively and then a constrained optimization to maximize productivity and minimize energy was carried out. The key findings of the current study can be summarized as follows:

- A novel carbon-based adsorbent, with a potential for pre-combustion CO_2 capture, was demonstrated to be stable under high-pressure, temperature, and moisture content. The stability of the adsorbent was proven by testing for over 11,650 cycles.
- The introduction of a steam purge provides the ability to increase adsorbent utilization, resulting in higher productivities.
- The combination of using detailed models, that provide insight into the movement of composition fronts, and multi-objective optimization algorithms, that provide an objective comparison of various cycles, was demonstrated to be an excellent tool for process design.
- An approach to calculate energy consumption by taking into account, the energy lost due to steam consumption in the process, compression of CO_2 and compression of product H_2 was proposed and used as a metric to compare various process configurations.
- The process optimization study using detailed models, demonstrated that three cycles can achieve US-DOE targets for CO_2 purity and

recovery. It was found that configuration F, a 10-step PSA cycle with three pressure equalization steps, achieved the lowest energy consumption of 95.7 kWh_e/tonne of CO_2 captured at a low productivity value (3.3 mol CO_2/m^3 adsorbent/s). Configuration D, which consisted of 1 pressure equalization and a co-current blowdown, was able to achieve a very high productivity of 7.4 mol CO_2/m^3 adsorbent/s, although at a high parasitic energy of 611.5 kWh_e/tonne of CO_2. Interestingly, although process D involved re-compression of H_2, it is possible to obtain higher productivities compared to process F, at a modest increase in energy consumption.

It is worth noting that some of the cycles suggested here have been implemented at a pilot-scale at the National Carbon Capture Centre, Alabama, USA [46]. The pilot-studies demonstrated the ability to capture > 90% CO_2 from a slip-stream. However, the demonstration study was implemented on an air-blown gasifier and hence, the product gas was heavily contaminated with N_2. The second phase of the study is now being carried out at the Sinopec refinery on an oxygen blown gasifier. This study which is currently on-going will implement some of the promising cycles discussed in this article and their results will be reported in a future study which will also include the integration of the PSA process with the steam systems.

Acknowledgements

Authors acknowledge funding from U.S. Department of Energy through Grant DE-FE0013105. Neither the U.S. Government nor any agency thereof, nor any of their employees, makes any warranty, express or implied, or assumes any legal liability or responsibility for the accuracy, completeness, or usefulness of any information, apparatus, product, or process disclosed, or represents that its use would not infringe privately owned rights. Reference herein to any specific commercial product, process, or service by trade name, trademark, manufacturer, or otherwise does not necessarily constitute or imply its endorsement, recommendation, or favoring by the U.S. Government or any agency thereof. The views and opinions of authors expressed herein do not necessarily state or reflect those of the U.S. Government or any agency thereof.

Appendix A. Supplementary material

Supplementary data associated with this article can be found, in the online version, at https://doi.org/10.1016/j.apenergy.2019.113624.

References

[1] IPCC, 2014, Climate Change 2014: Synthesis Report. Contribution of Working Groups I, II and III to the Fifth Assessment Report of the Intergovernmental Panel on Climate Change; 2014.
[2] IEA, CO_2 Capture and Storage: A Key Carbon Abatement Option; 2008.
[3] Li G, Xiao P, Webley P, Zhang J, Singh R, Marshall M. Capture of CO_2 from high humidity flue gas by vacuum swing adsorption with zeolite 13X. Adsorption 2008;14(2–3):415–22.
[4] Haines M, Kemper J, Davison J, Gale J, Singh P, Santos S. Assessment of emerging CO_2 capture technologies and their potential to reduce costs, TR 4, IEAGHG, December 2014.
[5] National Energy Technology Laboratory, Cost and Performance Baseline for Fossil Energy Plants; 2015.
[6] Bui M, Adjiman CS, Bardow A, Anthony EJ, Boston A, Brown S, et al. Carbon capture and storage (CCS): the way forward. Energy Environ Sci 2018;11(5):1062–176.
[7] Jansen D, Gazzani M, Manzolini G, van Dijk E, Carbo M. Pre-combustion CO_2 capture. Int J Greenh Gas Con 2015;40:167–87.
[8] Yan J, Zhang Z. Carbon capture, utilization and storage (CCUS). Appl Energy 2019;235:1289–99.
[9] Casas N, Schell J, Joss L, Mazzotti M. A parametric study of a PSA process for pre-combustion CO_2 capture. Sep Purif Technol 2013;104:183–92.
[10] Riboldi L, Bolland O, Ngoy JM, Wagner N. Full-plant analysis of a PSA CO_2 capture unit integrated in coal-fired power plants: post-and pre-combustion scenarios. Energy Procedia 2014;63:2289–304.
[11] Riboldi L, Bolland O. Evaluating pressure swing adsorption as a CO_2 separation technique in coal-fired power plants. Int J Greenh Gas Cont 2015;39:1–16.
[12] Agarwal A, Biegler LT, Zitney SE. Superstructure-based optimal synthesis of pressure swing adsorption cycles for precombustion CO_2 Capture. Ind Eng Chem Res 2010;49(11):5066–79.
[13] Liu Z, Green WH. Analysis of adsorbent-based warm CO_2 capture technology for integrated gasification combined cycle (IGCC) power plants. Ind Eng Chem Res 2014;53(27):11145–58.
[14] Luberti M, Friedrich D, Brandani S, Ahn H. Design of a H_2 PSA for cogeneration of ultrapure hydrogen and power at an advanced integrated gasification combined cycle with pre-combustion capture. Adsorption 2014;20(2–3):511–24.
[15] Moon D-K, Lee D-G, Lee C-H. H_2 pressure swing adsorption for high pressure syngas from an integrated gasification combined cycle with a carbon capture process. Appl Energy 2016;183:760–74.
[16] Moon D-K, Park Y, Oh H-T, Kim S-H, Oh M, Lee C-H. Performance analysis of an eight-layered bed PSA process for H_2 recovery from IGCC with pre-combustion carbon capture. Energy Convers Manag 2018;156:202–14.
[17] Zhu X, Shi Y, Cai N. Integrated gasification combined cycle with carbon dioxide capture by elevated temperature pressure swing adsorption. Appl Energy 2016;176:196–208.
[18] Zhu X, Shi Y, Li S, Cai N. Two-train elevated-temperature pressure swing adsorption for high-purity hydrogen production. Appl Energy 2018;229:1061–71.
[19] Ruthven DM, Farooq S, Knaebel KS. Pressure swing adsorption. Wiley VCH Publishers; 1994.
[20] Sircar S. Pressure swing adsorption. Ind Eng Chem Res 2002;41(6):1389–92.
[21] IEAGHG, The carbon capture project at air products' port arthur hydrogen production facility. 2018/05, December 2018.
[22] Casas N, Schell J, Pini R, Mazzotti M. Fixed bed adsorption of CO_2/H_2 mixtures on activated carbon: experiments and modeling. Adsorption 2012;18(2):143–61.
[23] Schell J, Casas N, Pini R, Mazzotti M. Pure and binary adsorption of CO_2, H_2, and N_2 on activated carbon. Adsorption 2012;18(1):49–65.
[24] Drage TC, Kozynchenko O, Pevida C, Plaza MG, Rubiera F, Pis J, et al. Developing activated carbon adsorbents for pre-combustion CO_2 capture. Energy Procedia 2009;1(1):599–605.
[25] Martín CF, Plaza MG, Pis J, Rubiera F, Pevida C, Centeno T. On the limits of CO_2 capture capacity of carbons. Sep Purif Technol 2010;74(2):225–9.
[26] Dietz SD, Alptekin G, Jayaraman A. High capacity carbon dioxide sorbent, Sept. 1 2015. US Patent 9,120,079.
[27] Rajendran A, Kariwala V, Farooq S. Correction procedures for extra-column effects in dynamic column breakthrough experiments. Chem Eng Sci 2008;63(10):2696–706.
[28] Chen Q, Rosner F, Rao A, Samuelsen S, Jayaraman A, Alptekin G. Simulation of elevated temperature solid sorbent CO_2 capture for pre-combustion applications using computational fluid dynamics. Appl Energy 2019;237:314–25.
[29] Haghpanah R, Majumder A, Nilam R, Rajendran A, Farooq S, Karimi IA, et al. Multiobjective optimization of a four-step adsorption process for postcombustion CO_2 capture via finite volume simulation. Ind Eng Chem Res 2013;52(11):4249–65.
[30] LeVeque RJ. Finite volume methods for hyperbolic problems. Cambridge University Press; 2002.
[31] van Leer B. Towards the ultimate conservative difference scheme. V. A second-order sequel to Godunov's method. J Comput Phys 1979;32(1):101–36.
[32] Krishnamurthy S, Rao VR, Guntuka S, Sharratt P, Haghpanah R, Rajendran A, et al. CO_2 capture from dry flue gas by vacuum swing adsorption: a pilot plant study. AIChE J 2014;60(5):1830–42.
[33] Hosseinzadeh Hejazi SA, Estupian Perez L, Pai KN, Rajendran A, Kuznicki SM. "Single-and dual-stage high-purity oxygen production using silver-exchanged titanosilicates (Ag-ETS-10)," Ind. Eng Chem Res 2018;57(27):8997–9008.
[34] Perez LE, Sarkar P, Rajendran A. Experimental validation of multi-objective optimization techniques for design of vacuum swing adsorption processes. Sep Purif Technol 2019;224:553–63.
[35] Haghpanah R, Nilam R, Rajendran A, Farooq S, Karimi IA. Cycle synthesis and optimization of a VSA process for postcombustion CO_2 capture. AlChE J 2013;59(12):4735–48.
[36] Rajagopalan AK, Avila AM, Rajendran A. Do adsorbent screening metrics predict process performance? A process optimisation based study for post-combustion capture of CO_2. Int J Greenh Gas Cont 2016;46:76–85.
[37] Hosseinzadeh Hejazi SA, Estupian Perez L, Rajendran A, Kuznicki S. Cycle development and process optimization of high-purity oxygen production using silver-exchanged titanosilicates. Ind Eng Chem Res 2017;56(19):5679–91.
[38] Pai KN, Baboolal JD, Sharp DA, Rajendran A. Evaluation of diamine-appended metal-organic frameworks for post-combustion CO_2 capture by vacuum swing adsorption. Sep Purif Technol 2019;211:540–50.
[39] Verma MK. Fundamentals of Carbon Dioxide-Enhanced Oil Recovery (CO_2-EOR) – A supporting document of the assessment methodology for hydrocarbon recovery using CO_2-EOR associated with carbon sequestration. U.S. Department of the Interior and U.S. Geological Survey; 2015.
[40] DECARBit. European best practice guidelines for assessment of CO_2 capture technologies. European Commission; 2010.
[41] Span R, Wagner W. A new equation of state for carbon dioxide covering the fluid region from the triple point temperature to 1100 K at pressures up to 800 MPa. J Phys Chem Ref Data 1996;25(6):1509–96.
[42] Ulrich GD, Vasudevan PT. Chemical engineering process design and economics: a practical guide. Durham, New Hampshire: Process Publishing; 2004.
[43] Chien SF. Empirical correlations of saturated steam properties vol. 7. Society of Petroleum Engineers; 1992.
[44] Affandi M, Mamat N, Kanafiah SNAM, Khalid NS. Simplified equations for saturated steam properties for simulation purpose. Procedia Eng 2013;53:722–6.
[45] Deb K, Pratap A, Agarwal S, Meyarivan T. A fast and elitist multiobjective genetic algorithm: NSGA-II. IEEE Trans Evol Comput 2002;6(2):182–97.
[46] Alptekin G, Jayaraman A, Cates M, Bonnema M, Gribble D, Dippo J. Pilot testing of a highly efficient pre-combustion sorbent-based carbon capture system. <https://www.netl.doe.gov/sites/default/files/netl-file/G-Alptekin-TDAR-Pre-Combustion-Sorbent.pdf> [accessed: 2019-06-18].